Nanoscale

Accepted Manuscript

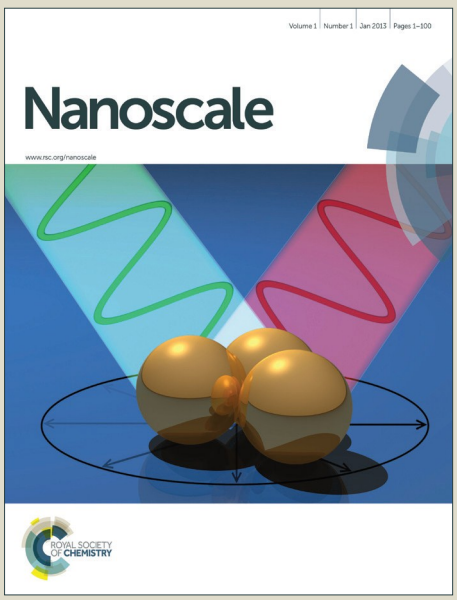

This is an *Accepted Manuscript*, which has been through the Royal Society of Chemistry peer review process and has been accepted for publication.

Accepted Manuscripts are published online shortly after acceptance, before technical editing, formatting and proof reading. Using this free service, authors can make their results available to the community, in citable form, before we publish the edited article. We will replace this *Accepted Manuscript* with the edited and formatted *Advance Article* as soon as it is available.

You can find more information about *Accepted Manuscripts* in the Information for Authors.

Please note that technical editing may introduce minor changes to the text and/or graphics, which may alter content. The journal's standard Terms & Conditions and the Ethical guidelines still apply. In no event shall the Royal Society of Chemistry be held responsible for any errors or omissions in this *Accepted Manuscript* or any consequences arising from the use of any information it contains.

ROYAL SOCIETY OF CHEMISTRY

www.rsc.org/nanoscale

Facile Preparation of Uniform $FeSe_2$ Nanoparticles for PA/MR Dual-Modal Imaging and Photothermal Cancer Therapy

Tingting Fu[1], Yuyan Chen[2], Jiali Hao[2], Xiaoyong Wang[3], Gang Liu[3], Yonggang Li[1*], and Zhuang Liu[2], Liang Cheng[2*]

[1]Department of Radiology the First Affiliated Hospital of Soochow University Suzhou, Jiangsu, 215006, China

[2]Institute of Functional Nano & Soft Materials (FUNSOM), Collaborative Innovation Center of Suzhou Nano Science and Technology, Soochow University, Suzhou, Jiangsu 215123, China

[3]Center for Molecular Imaging and Translational Medicine, School of Public Health, Xiamen University, Xiamen 361005, China

Email: lcheng2@suda.edu.cn; liyonggang224@163.com;

Abstract:

Recently, magnetic photothermal nanomaterials have emerged as a new class of bio-nanomaterials for application in cancer diagnosis and therapy. Hence, we developed a new kind of magnetic nanomaterials, iron diselenide ($FeSe_2$) nanoparticles, for multimodal imaging-guided photothermal therapy (PTT) to improve the efficacy of cancer treatment. By controlling the reaction time and temperature, $FeSe_2$ nanoparticles were synthesized by a simple solution-phase method. After modification with polyethylene glycol (PEG), the obtained $FeSe_2$-PEG nanoparticles showed high stability under various physiological conditions. $FeSe_2$-PEG could serve as a T2-weight magnetic resonance (MR) imaging contrast agent because of their strong superparamagnetic property, with its r_2 relaxivity determined to be 133.38 $mM^{-1}S^{-1}$, a value higher than that of the clinically used Feridex.

Nanoscale Accepted Manuscript

On the other hand, with high absorbance in the near-infrared (NIR) region, $FeSe_2$-PEG also appeared to be a useful contrast agent for photoacoustic imaging (PA) as well as an effective photothermal agent for PTT cancer treatment, as demonstrated in our animal tumor model experiments. Moreover, long-term toxicity tests have proven that $FeSe_2$-PEG nanoparticles after systematic administration rendered no appreciable toxicity to the treated animals, and could be gradually excreted from major organs of mice. Our work indicates that $FeSe_2$-PEG nanoparticles would be a new class of theranostic agent promising for application in bioimaging and cancer therapy.

Keywords: $FeSe_2$ nanoparticles, Magnetic resonance imaging (MRI), Photoacoustic imaging, Photothermal therapy, Long-term toxicity

1. Introduction

Photothermal therapy (PTT), as a noninvasive treatment technique for cancer therapy, employs near-infrared (NIR) photoabsorbers to convert light energy into thermal energy to burn tumor cells[1, 2]. Compared with traditional cancer therapy methods, PTT exhibits high specificity, great efficiency, and few side effects[2, 3]. During the past few years, many inorganic and organic nanoparticles have been explored as PTT agents, such as Au-based nanomaterials[1, 4, 5], carbon-based nanomaterials[6, 7], Cu-based nanomaterials[8, 9], palladium nanosheets[10], transition-metal dichalcogenides[11-13], conjugated polymers[14-16], and nano-complexes containing small organic NIR dyes[17, 18]. Meanwhile, imaging-guided photothermal cancer ablation has attracted intensive interests[11, 19-25]. Under the guidance of imaging, people can identify the location and size of tumors and the presence of photo-absorbing agents in the tumor before therapy, monitor the treatment procedures in real-time during therapy, and assess the effectiveness after therapy. Recently, numerous imaginable

Nanoscale Accepted Manuscript

photothermal agents have been successfully synthesized[2, 11, 26-30].

Among the various imaging techniques, magnetic resonance (MR) imaging is one of the most powerful diagnostic technologies due to its high temporal and spatial resolution, and unlimited tissue penetration[31]. Therefore, it would be a wise protocol to integrate MRI and PTT into a single probe, namely magnetic photothermal nanoprobe, which offers the possibility of combining the contrast-based volume imaging and photothermal cancer therapy. In recent years, several types of magnetic photothermal nanoparticles, such as Fe_3O_4@Au, Fe_3O_4@$Cu_{2-x}S$, and Fe_5C_2@C core-shells nanostructures, have emerged as multifunctional contrast agents for imaging-guided PTT.[8, 20, 32, 33]. However, for most of the abovementioned agents, two kinds of functional nanostructures are constructed together: one for MR imaging, the other for PTT, thus requiring relatively complicated nanostructure engineering during synthesis. Recently, FeS nanoplates and Co_9Se_8 nanoparticles with single components have been reported as new magnetic photothermal agents[34, 35]. However, while FeS nanoplates reported in our recent work showed rather irregular morphology / sizes and appeared to be relatively unstable against oxidization in aqueous solutions, Co_9Se_8 nanoparticles contain Co element, which arise concerns regarding their potential long-term toxicity. There is still a great demand to develop new multifunctional theranostic agents that integrate MR imaging and PTT functionalities into a single nano-platform, with great performances and low toxicities.

Iron selenide (FeSe, and $FeSe_2$) has a direct band gap of 1.23 eV and an absorption coefficient of 5×10^5 cm^{-1} for $\lambda < 800$ nm. $FeSe_2$ is also known to have indirect band gaps of 0.86 and 0.67 eV in the marcasite and pyrite phases[36-38] , respectively. Taken together, iron selenide nanoparticles may be used as photothermal agents due to high absorbance in the NIR region. Such a possibility, however, has not yet been explored to our best knowledge. In this work, $FeSe_2$ nanoparticles with

Nanoscale Accepted Manuscript

uniform sizes were synthesized via a simple solution-phase method and then functionalized with poly (acrylic acid) (PAA) and polyethylene glycol (PEG) (**Figure 1a**). The obtained PEGylated $FeSe_2$ ($FeSe_2$-PEG) nanoparticles showed strong NIR absorbance and intrinsic superparamagnetism. The r2 relaxivity of $FeSe_2$-PEG was determined to be 133.38 mM^{-1} S^{-1}, which appeared to be much higher than that of clinically approved T_2-contrast agents (72 mM^{-1} S^{-1} for ferumoxsil and 98.3 mM^{-1} S^{-1} for ferumoxide)[39]. In the meanwhile, the NIR absorbance property of $FeSe_2$-PEG was applied to in vivo photoacoustic imaging (PA) and photothermal therapy (PTT) in mouse tumor model. Importantly, systematic *in vivo* toxicology evaluation demonstrated no appreciable toxicity of these nanoparticles, which could be gradually excreted overtime upon intravenous injection. Our work for the first time demonstrated that $FeSe_2$ nanoparticles may have great potential as a safe, multi-functional theranostic agent for imaging guided photothermal treatment of cancer.

2. Experimental section

Synthesis of $FeSe_2$ nanoparticles: All materials were obtained from Sigma-Aldrich, unless specifically indicated. For the synthesis of $FeSe_2$ nanoparticles, oleylamine (OM, 15 mL) and 1-octadecene (ODE, 10 mL) were added into a three-necked flask (50 mL) at room temperature. The mixed solution was heated to 120°C under nitrogen protection and kept at that temperature for 30 min. Then $FeCl_2 \cdot 4H_2O$ (1 mmol) powder was added into the mixture solution followed by vigorous magnetic stirring for 30 min. Selenium powder (2 mmol) dissolved in 4 mL OM was then injected into the flask and stirred for 10 min. Afterwards, the temperature of the mixture was rapidly raised to 150°C and kept there for another 30 min under the production of nitrogen. After the reaction, the products were cooled to room temperature. To precipitate the generated $FeSe_2$ nanoparticles, excess

Nanoscale Accepted Manuscript

ethanol was added. $FeSe_2$ nanoparticles were then collected by centrifugation and washed repeatedly with hexane and ethanol. The final product was dispersed in ethanol and stored at 4°C for future use. Ultra-small iron oxide nanoparticles synthesized by the previous report were used as the control[40].

Functionalization of $FeSe_2$ nanoparticles: Poly (acrylic acid) (PAA, ~1800 MW, Sigma-Aldrich) aqueous solution was added slowly into the ethanol solution of $FeSe_2$ under ultrasonication for 30 min. After the mixture was stirred for 6 h, the water-soluble PAA modified $FeSe_2$ nanoparticles were obtain after centrifugation to remove excess PAA and ethanol at 14800 rpm for 5 min, and then re-dispersed in water. Lastly, in order to obtained PEG coated nanoparticles, mPEG-NH_2 (MW = 5000, Biomatrik, Jiaxing, China) was added into the $FeSe_2$-PAA solution under ultrasonication for 30 min. Two proportions of 5 mg of N-(3-dimethylaminopropyl-N'-ethylcarbodiimide) hydrochloride (EDC, Fluka Inc.) was added into the solution. The reaction was stirred at room temperature overnight. The yielded $FeSe_2$-PEG solution was purified by centrifugation (14800 rpm, 5min) to remove large aggregates and stored at 4°C for future experiments.

Characterization: Transmission electron microscopy (TEM) images of the nanoparticles were obtained using a FEI Tecnai F20 transmission electron microscope equipped with an energy dispersive spectroscope (EDX) at an acceleration voltage of 200 kV The phase and crystallography of the products were characterized by using a PANalytical X-ray diffractometer equipped with Cuka radiation (λ=0.15406 nm). A scanning rate of 0.05 $^{o}s^{-1}$ was applied to record the pattern in the 2θ range of 20-80°. UV-vis-NIR spectrum of $FeSe_2$-PEG was obtained with PerkinElmer Lambda 750 UV-vis-NIR spectrophotometer. The hydrodynamic diameters and zeta potentials of $FeSe_2$-PAA and $FeSe_2$-PEG nanoparticles were determined by a Zetasizer Nano-ZS (Malvern Instruments, UK).

Nanoscale Accepted Manuscript

T2-weighted images of $FeSe_2$-PEG in different concentrations were scanned under a 3T clinical MRI scanner at room temperature. After the T2-weighted MR images were acquired, the signal intensity was measured by a manually drawn region-of-interest for each sample. Relaxation rates R2 (R2 =1/T2) were calculated from T2 values with different iron concentrations.

Cell culture experiments: 4T1 murine breast cancer cells, HeLa human cervical cancer cells, and 293T human embryo kidney cells were originally obtained from American Type Culture Collection (ATCC), and cultured in standard cell media recommended by American type culture collection (ATCC) supplemented with 10% FBS and 1% penicillin/streptomycin at 37°C in a 5% CO_2-containing atmosphere.. All cell culture related reagents were purchased from HyClone. For cell viability test, cells were seeded into 96 well plates at $5*10^4$ cells per well and then incubated with different concentrations of $FeSe_2$ -PEG for 24h. Relative cell viabilities were determined by a standard cell viability assay using 3-(4, 5-dimethylthiazol-2-yl)-2, 5-diphenyltetrazolium bromide (MTT).

***In vitro* PTT:** 4T1 cancer cells seeded in 96-well plates incubated with or without $FeSe_2$ -PEG (0.1 mg/mL) for 4 h and then irradiated by an 808-nm laser at different power densities (0, 0.1, 0.3, 0.5, 0.8 W/cm ^{2}) for 5 min . The cells were then incubated at 37 ^{o}C for additional 24 h before the standard MTT assay. The cells irradiated by different power densities (0, 0.3, 0.5, 0.8 W/cm ^{2}) were co-stained with Calcein AM (green, live cells) and propidium iodide (PI) (red, dead cells) for 30 min and then washed with PBS. Fluorescence microscopic images of cells were taken using an Olympus fluorescent microscope.

Tumor model: We acquired female Balb/c mice from Nanjing Peng Sheng Biological Technology Co. Ltd, which were utilized to abide by protocols approved by Soochow University

Nanoscale Accepted Manuscript

Laboratory Animal Center. To generated the 4T1 tumors murine model, $2*10^6$ cells in 40 μL serum-free RMPI-1640 medium were subcutaneously injected into the back of each mouse.

***In vivo* MR and PA bimodal imaging:** 4T1 tumor-bearing mice were intratumorally (i.t.) injected with $FeSe_2$-PEG (40 μL, 2 mg/mL) and imaged with a preclinical photoacoustic computed tomography scanner (Endra Nexus 128, Ann Arbor, MI). The MR images were acquired before and after intratumorally injection with $FeSe_2$-PEG (40 μl, 2 mg/ml) on a 3.0 T clinical magnetic resonance (MR) scanner (GE healthcare, USA) equipped with a small animal coil. Representative imaging parameters for the T2-weighted images were as follows: repetition time (TR) = 2000 ms, echo time (TE) = 106.4 ms, slice thickness= 2.0 mm, slice spacing= 0.2 mm, matrix= 224×192 pixels, field of view (FOV) =10 cm×10 cm. Region-of-interest in the tumor area of each mouse was selected by manual drawing to measure the signal intensity of tumors from the T2-weighted MR images.

***In vivo* PTT experiments:** Three groups of 4T1 tumor-bearing mice were intratumorally injected with the same concentration of $FeSe_2$-PEG (40 μL of 2 mg/mL, dose =4 mg/kg). 0.5 h later, the mice were exposed to the 808 nm laser with different laser power densities (0.3, 0.5, 0.8W/cm^2) for 5 min. Tumor-bearing mice *i.t* injected with the same volume of saline were also exposed to the 808-nm laser (0.8W/cm^2) as the control. An Infrared (IR) thermal imaging camera (IRS E50 Pro Thermal Imaging Camera) was used to monitor the tumor temperature. Tumor sizes were recorded by a caliper every other day after treatment to calculate the tumor volume: V= (tumor length) × (tumor width) ^{2} /2. Relative tumor volumes were calculated as V/V_0 (V_0 was the tumor volume measured at the beginning of treatment). Mice with tumors larger than 1000 mm^3 should be euthanized according to the standard animal protocol.

Long-term toxicity study: The blood sample and major organs/tissues were taken from mice

Nanoscale Accepted Manuscript

after intravenous injection of $FeSe_2$-PEG (a dose of 20 mg/ kg) at 1 day, 7 days, 14 days and 30 days post-injection (p.i.) (four mice per group). Other four mice without injection were used as the control group The collected blood samples were tested in Shanghai Research Center for Biomodel Organism to obtain serum chemistry data and complete blood panel. Part of the harvested major organs/tissues were fixed in 4% formalin, paraffin embedded, sectioned and stained with hematoxylin & eosin (H&E), and then imaged by a digital microscope (Leica QWin).

***In vivo* biodistribution study:** Detection of iron levels in organs of the above five groups of mice could reveal the *in vivo* biodistribution of $FeSe_2$-PEG nanoparticles. After weighing organ samples including liver, spleen, kidney, heart, lung, stomach, intestine, skin, muscle, and bone, we put them into aqua regia, which was heated at 200°C for 2 h. Each of those dissolved tissue sample was then diluted to 10 mL by deionized water. Inductively coupled plasma atomic emission spectroscopy (ICP-AES, Vista Mpx 700-ES) was used to determine the Fe concentrations in the obtained solutions. Untreated mice were used as the blank control.

3. Results and discussion

In our experiments, high-quality $FeSe_2$ nanoparticles with uniform sizes and morphology were synthesized from iron (II) chloride and selenium in a mixed solvent of oleyamine (OM) and 1-octadecene (ODE) under N_2 atmosphere via a simple solution-phase method. During the reaction course, the iron (II) precursor solution gradually turned into pale-yellow, probably because of the reaction between $FeCl_2$ and OM that gave rise to a Fe-OM complex. When the solvent temperature reached 150 ^{o}C, selenium dissolved in OM was injected into the reaction solution. Upon injection of the selenium source, the solution color gradually turned into black, suggesting the formation of $FeSe_2$.

Nanoscale Accepted Manuscript

Transmission electron microscopy (TEM) image revealed that the diameters of most as-made $FeSe_2$ nanoparticles were in the range of 8~10 nm (**Fig. 1b**). The XRD pattern of obtained nanoparticles (**Fig. 1c**) suggested the orthorhombic structure of $FeSe_2$ (JCPDS card, No.21-0432). No peaks of any other phases were detected, indicating the high purity of the final product. The mapping of $FeSe_2$ nanoparticles under high-angle annular detector dark-field scanning transmission electron microscopy (HADDF-STEM) showed that the nanoparticles were constituted by Fe and Se elements (**Fig. 1d**). The EDX pattern provided the elemental ratio, and revealed that those $FeSe_2$ nanoparticles contained 32.9% of Fe and 67.1% of Se by the atom percentage (**Fig. 1e**). Note that the C, O, and Cu elements in the spectrum were from carbon-coated copper TEM grids.

In order to understand the formation of $FeSe_2$ nanoparticles in detail, we studied the influence of reaction conditions on the shape and size of products systematically. **Figure 2** shows the TEM and XRD spectra of $FeSe_2$ samples prepared with different reaction time. We did not see a great influence of reaction time on the growth of $FeSe_2$ nanoparticles. When the reaction time was shortened to 10 min or prolonged to 60 min, we still obtained pure $FeSe_2$ nanoparticles from the XRD results (**Fig. 2a&2c**). Then the effect of reaction temperature was also investigated (**Fig. 2b&2d**). From these TEM images (**Fig 2a&2b, Supporting Figure S1**), it can be seen that we could only obtain uniform nanoparticles at temperature lower than 150 ^{o}C. When the temperature increased to be above 180 ^{o}C, the obtained nanoparticles would be aggregated and grown to larger sizes. Aggregated $FeSe_2$ nanorods would be formed if the temperature was increased to 240 ^{o}C. Based on the above experimental results, we summarized the effect of reaction parameters and proposed a mechanism for the nucleation and growth of $FeSe_2$ nanoparticles as follows. Firstly, the reaction time had little effect on the morphology of the products, indicating that the nucleation and growth of $FeSe_2$ nanocrystals

Nanoscale Accepted Manuscript

was a rapid a process that is finished within a few minutes. Secondly, the reaction temperature was an important factor influencing the nucleation and growth of $FeSe_2$ nanocrystals. The probable mechanism was that $FeSe_2$ nuclei were quickly formed upon injection of Se-OM into Fe-OM complex, and grown to a certain size over time. However, the sizes of $FeSe_2$ nanoparticles were controlled because their surface was protected by OM ligands. As the temperature increases, the interaction between OM and Fe becomes weaker, leading to the formation of $FeSe_2$ nanoparticles with larger sizes and broader size distribution. The temperature at 150 ^{o}C was found to be the most suitable for the synthesis of high-quality $FeSe_2$ nanocrystals with uniform sizes.

To obtain water soluble $FeSe_2$ nanoparticles, we functionalized their surface with PAA. The obtained PAA-$FeSe_2$ nanoparticles, although could be dispersed in water, would aggregate in salt solutions. Therefore, a biocompatible hydrophilic polymer, mPEG-NH_2 (5 kDa), was applied to coat $FeSe_2$-PAA via amide formation to obtain PEGylated $FeSe_2$ nanoparticles. Dynamic light scattering (DLS) was used to determine the size of $FeSe_2$-PEG in various physiological solutions including water, phosphate buffer saline (PBS), RMPI-1640 cell medium and fetal bovine serum (FBS) (**Supporting Figure S2**). The obtained PEGylated $FeSe_2$ had wonderful stability in various physiological solutions (**Fig. 3a, inset**). Even at lower pH value solution (pH=5.0), the PEGylated $FeSe_2$ nanoparticles still showed high stability (**Supporting Figure S3**).

The optical properties of $FeSe_2$-PEG were then studied. Compared with dopamine (DA) modified iron oxide (Fe_3O_4) nanoparticles (diameter ~ 6 nm) synthesized by the high-temperature method (Supporting Figure S4), $FeSe_2$-PEG exhibited much stronger broad band absorbance in the NIR region (Fig. 3a). The weight extinction coefficient of $FeSe_2$ was measured to be 32.6 L $g^{-1}cm^{-1}$ at 808 nm, which was much higher than that of GO (5.94 L $g^{-1}cm^{-1}$)[41], reduced graphene oxide (GO)

Nanoscale Accepted Manuscript

(21.1 L $g^{-1}cm^{-1}$)[3], MoS_2 (29.8 L $g^{-1}cm^{-1}$)[42], and WS_2 (23.8 L $g^{-1}cm^{-1}$)[11]. As expected, $FeSe_2$-PEG nanoparticles had good photothermal property under 808-nm NIR laser irradiation, which could induce concentration-dependent temperature increases for aqueous solutions of $FeSe_2$-PEG (**Fig. 3b, Supporting Figure S5**). The photothermal stability of $FeSe_2$-PEG was also tested. It was found that $FeSe_2$-PEG remained to be a rather robust photothermal heater after five cycles of NIR laser-induced heating (808-nm laser at 0.8 W/cm^2, 3 min laser irradiation for each cycle) **(Supporting Figure S6)**. No significant absorbance change after exposure to the NIR laser for as long as 30 min was noticed, demonstrating the excellent photothermal stability of $FeSe_2$-PEG nanoparticles. The strong photothermal performance and excellent photostability of $FeSe_2$-PEG nanoparticles make them an encouraging nano-agent for PTT cancer treatment.

We next looked into the magnetic properties of $FeSe_2$-PEG. The superparamagnetic property of $FeSe_2$-PEG was illustrated by the absence of a hysteresis loop in the field-dependent magnetization measurement (**Fig. 3c**). To investigate the MR contrasting performance of $FeSe_2$-PEG, a 3.0 T MR instrument was used for T2-weighted MR imaging. As shown in **Fig. 3d&3e**, the T2-weighted imaging signals of $FeSe_2$-PEG and Fe_3O_4-DA solutions gradually reduced with the increase of their respective concentrations. Under the same Fe concentration, the images of $FeSe_2$-PEG solutions appeared to be much darker than those of Fe_3O_4-DA solutions. The r2 relaxivity of $FeSe_2$-PEG was measured to be 133.38 mM^{-1} s^{-1} based on the Fe concentration, which was much higher than that of Fe_3O_4-DA (88.99 mM^{-1} s^{-1}) (**Fig. 3d**). Clearly, $FeSe_2$-PEG can be used as an effective T2 MR contrast agent.

Because potential toxicity is crucial for further biological applications, we studied the in vitro toxicity of $FeSe_2$-PEG towards different cells lines. 4T1 murine breast cancer cells, HeLa human

Nanoscale Accepted Manuscript

cervical cancer cells, and 293T human embryo kidney cells were incubated with different concentrations of $FeSe_2$-PEG for 24 h. The standard methyl thiazolyl tetrazolium (MTT) assay was then used to determine their relative viabilities. $FeSe_2$-PEG nanoparticles had no obvious toxicity to these three cell lines (**Fig. 4a**), even at the highest concentration of 100 μg/mL. We then used 4T1 cancer cells to verify the *in vitro* PTT effect of $FeSe_2$-PEG nanoparticles. After incubation with $FeSe_2$-PEG at the concentration of 50 μg/mL for 4 h, 4T1 cells were then exposed to an 808-nm laser. With the increase of laser power density, the remained cell viabilities reduced accordingly, as revealed by both MTT assay and Calcine AM & propidium iodide (PI) co-staining assay (**Fig. 4b&4c**). Almost all cancer cells were killed after laser irradiation at 0.8 W/cm^2 for 5 min. In contrast, cells without $FeSe_2$-PEG nanoparticles incubation were not affected even after laser exposure at the highest power density. These results demonstrated the potential of $FeSe_2$-PEG nanoparticles as an efficiency photothermal agent for localized ablation of cancer cells under NIR laser irradiation.

Inspired by the high r2 value of $FeSe_2$-PEG, we next applied $FeSe_2$-PEG as a T2- MR contrast agent to study its *in vivo* imaging contrast capability. Before and after intratumorous (*i. t.*) injection with $FeSe_2$-PEG (40 μL of 2 mg/mL), the tumor-bearing mice were imaged by the 3.0 T clinical MR scanner equipped with a small animal imaging coil. Compared with that before nanoparticles injection, we found a remarkable darkened effect in the tumors of mice after nanoparticle injection (**Fig. 5a&5b, 5e**).

Photoacoustic imaging (PA), which has attracted significant interests in recent years, is developed based on the photoacoustic effect of light-absorbers and offers remarkably increased imaging depth and spatial resolution compared to traditional *in vivo* optical imaging[41, 43-45]. The high NIR absorbance of $FeSe_2$-PEG would make it a good PA imaging contrast agent. Before and after

Nanoscale Accepted Manuscript

injecting $FeSe_2$-PEG to the tumor-bearing mice, remarkably enhanced signals could be seen in the tumor area (**Fig. 5c-5e**). Thus, it is possible to use $FeSe_2$-PEG as a multimodal imaging probe. The sensitivity and spatial resolution is the limitations of MR imaging though it can image the whole body without the tissue depth limit. Opposite to MR imaging, PA imaging, which is not capable of whole-body imaging, performs well in spatial resolution and would be able to illustrate the detailed distribution of nanoparticles inside the tumor. Taking those advantages of the two imaging modailities together, more valuable information may be obtained for planning and guiding therapeutic actions.

Next, we used $FeSe_2$-PEG as a photothermal agent for *in vivo* cancer treatment. Three groups of 4T1 tumor-bearing mice were *i.t.* injected with the same concentration of $FeSe_2$-PEG (40 μL of 2 mg/mL, dose =4 mg/kg). After 0.5 h, the mice were exposed to the 808-nm laser with different power densities (0.3, 0.5, 0.8W/cm^2) for 5 min. Tumor-bearing mice *i.t* injected with the same volume of saline were also exposed to the 808-nm laser (0.8W/cm^2) as the control. An Infrared (IR) thermal imaging camera was used to monitor the tumor temperatures under laser irradiation. With the increase of laser power density, the temperature of the tumor surface obviously increased (**Fig. 6a**). When exposed to the laser at 0.8 W/cm^2, the highest temperature of the tumor injected with $FeSe_2$-PEG reached to ~63.4 ^{o}C within 5 min, which would be high enough to ablate tumors *in vivo*. In contrast, the temperature of tumors without $FeSe_2$-PEG injection showed no significant increase under laser irradiation at the same irradiation condition.

The PTT efficacy with $FeSe_2$-PEG nanoparticles to ablate tumors was then studied. Mice bearing 4T1 tumors (volume ~ 50 mm^3) were randomly divided into four groups (n =4 per group): (1) untreated control, (2) 808 nm laser only (0.8 W/cm^2, 5 min) (3) $FeSe_2$-PEG nanoparticles i.t injection

Nanoscale Accepted Manuscript

(dose =4 mg/kg), (4) $FeSe_2$-PEG nanoparticles i.t injection and irradiated with 808 nm light (PTT) (dose =4 mg/kg, 0.8 W/cm^2, 5 min). It was found that tumors after injection of $FeSe_2$-PEG followed by laser irradiation were eradicated without recurrence within 40 days (**Fig. 6b&6c**). The tumors of all the other groups, by comparison, did not show any trend of growth inhibition (**Supporting Figure S7**). Therefore, our results demonstrated the excellent *in vivo* cancer therapeutic effect of the PTT mediated by $FeSe_2$-PEG.

Finally, to study the long-term biodistribution and toxicity of $FeSe_2$-PEG nanoparticles *in vivo*, healthy Balb/c mice were intravenously injected with $FeSe_2$-PEG (dose = 20 mg/kg) and sacrificed at 1 day, 7 days, 14 days and 30 days p.i. to collect blood as well as main organs and tissues. Those organs were cut into two halves, with one set of organs used for biodistribution study, in which those organs were solubilized with aqua regia. Then we used inductively coupled plasma atomic emission spectrometry (ICP-AES) to determine the total amount of Fe in each measured organ. Iron contents mainly cumulated in liver and spleen (RES) organs for the reason of phagocytic function of macrophages in reticuloendothelial system (RES) (**Fig. 7a**). Notably, a persistent decrease of iron levels in all measured major organs was observed, indicating time-dependent clearance of those nanoparticles from those organs. Prussia blue staining of spleen slices also evidenced the gradual clearance of iron from mice i.v. injected with $FeSe_2$-PEG (**Supporting Figure S8**). Therefore, we concluded that $FeSe_2$-PEG could be effectively eliminated from the treated animals.

For toxicology study, blood chemistry and blood routine examination were conducted with the blood samples of the above mice. Liver and kidney are principal organs for accumulation, metabolism and excretion of nanoparticles. In blood chemistry analysis, alkaline phosphatase (ALP),

Nanoscale Accepted Manuscript

aspartate aminotransferase (AST) and alanine aminotransferase (ALT) reflecting liver function, as well as urea nitrogen (BUN), a specific serological marker for kidney function, were selected. All the mention-above detection indexes remained within the normal ranges (**Fig. 7b&c**), suggesting that intravenous injection of $FeSe_2$-PEG had no major hepatotoxic effects and renal toxicity even at the dose of 20 mg/kg. In the meanwhile, the blood routine indexes including white blood cells (WBC), red blood cells (RBC), platelet (PLT), mean corpuscular hemoglobin (MCH), mean corpuscular volume (MCV), hematocrit (HCT), hemoglobin (HGB), and mean corpuscular hemoglobin concentration (MCHC), in $FeSe_2$-PEG treated mice were all measured to be comparable to that of the untreated healthy mice (**Fig. 7d-6k**). Histological examination was also conducted by H&E staining of major organ slices (liver, spleen, kidney, heart and lung) of the above five group of mice (**Supporting information, Figure S9**). We did not notice obvious morphology damage on organs. Taken together, $FeSe_2$-PEG nanoparticles upon intravenous injection showed no appreciable toxic effect to the treated animals within 30 days at the tested dose.

4. Conclusions

In this work, PEGylated $FeSe_2$ nanoparticles are developed as a new magnetic photothermal agent, which is featured with high r2 relaxivity and strong NIR-absorbance. The r2 relaxivity of $FeSe_2$-PEG is determined to be 133.38 mM^{-1} S^{-1}, much higher than that of clinically approved T_2-contrast agents. In the meanwhile, the weight extinction coefficient of $FeSe_2$ is measured to be 32.6 L $g^{-1}cm^{-1}$ at 808 nm, also much higher than that of many commonly used inorganic photothermal nano-agents (e.g. gold nanorods, graphene oxide, reduced graphene oxide, CuS, MoS_2, etc.). Compared with our previous reported FeS nanoflakes[34], our synthesized $FeSe_2$ nanoparticles

Nanoscale Accepted Manuscript

show rather uniform size / morphology, and appear to be stable in aqueous solutions against oxygen-induced oxidization. Utilizing the magnetic and optical properties of $FeSe_2$-PEG, *in vivo* MR/PA dual modal imaging and photothermal cancer therapy were carried out. Furthermore, those nanoparticles after intravenous injection could be gradually excreted, reaching to a nearly complete clearance in 30 days, without showing noticeable toxicity to treated mice at a dose of 20 mg/kg. Due to their excellent imaging ability, effective PTT effect and low toxicity, $FeSe_2$-PEG nanoparticles could be used as a new theranostic agent with multiple functionalities integrated within a single component.

Acknowledgements

L. Cheng was supported by the National Natural Science Foundation of China (51302180, 51572180) and a Post-doctoral science foundation of China (2013M531400, 2014T70542). L. Cheng also acknowledges the Collaborative Innovation Center of Suzhou Nano Science and Technology (Nano-CIC) for the fellowship of "Young Scientists Overseas Exchanges And Cooperation Program". Z. Liu was supported by the National "973" Program of China (2012CB932601), and a Project Funded by the Priority Academic Program Development of Jiangsu Higher Education Institutions. Y.G. Li was supported by the National Natural Science Foundation of China (81171394, 81171392), and a Project Funded by the Priority Academic Program Development (PAPD) of Jiangsu Higher Education Institutions.

Nanoscale Accepted Manuscript

References:

1. X. Huang, I. H. El-Sayed, W. Qian and M. A. El-Sayed, *J. Am. Chem. Soc.*, 2006, **128**, 2115-2120.
2. L. Cheng, C. Wang, L. Feng, K. Yang and Z. Liu, *Chem. Rev.*, 2014, **114**, 10869-10939.
3. J. T. Robinson, S. M. Tabakman, Y. Liang, H. Wang, H. Sanchez Casalongue, D. Vinh and H. Dai, *J. Am. Che. Soc.*, 2011, **133**, 6825-6831.
4. A. M. Alkilany, L. B. Thompson, S. P. Boulos, P. N. Sisco and C. J. Murphy, *Adv. Drug Delivery Rev.*, 2012, **64**, 190-199.
5. R. Lv, P. Yang, F. He, S. Gai, G. Yang, Y. Dai, Z. Hou and J. Lin, *Biomaterials*, 2015, **63**, 115-127.
6. K. Yang, L. Feng, X. Shi and Z. Liu, *Chem. Soc. Rev.*, 2013, **42**, 530-547.
7. X. Liu, H. Tao, K. Yang, S. Zhang, S.-T. Lee and Z. Liu, *Biomaterials*, 2011, **32**, 144-151.
8. Q. Tian, J. Hu, Y. Zhu, R. Zou, Z. Chen, S. Yang, R. Li, Q. Su, Y. Han and X. Liu, *J. Am. Chem. Soc.*, 2013, **135**, 8571-8577.
9. M. Zhou, R. Zhang, M. Huang, W. Lu, S. Song, M. P. Melancon, M. Tian, D. Liang and C. Li, *J. Am.Chem. Soc.*, 2010, **132**, 15351-15358.
10. X. Huang, S. Tang, X. Mu, Y. Dai, G. Chen, Z. Zhou, F. Ruan, Z. Yang and N. Zheng, *Nat. Nanotechnol.*, 2011, **6**, 28-32.
11. L. Cheng, J. Liu, X. Gu, H. Gong, X. Shi, T. Liu, C. Wang, X. Wang, G. Liu and H. Xing, *Adv. Mater.s*, 2014, **26**, 1886-1893.
12. S. Wang, X. Li, Y. Chen, X. Cai, H. Yao, W. Gao, Y. Zheng, X. An, J. Shi and H. Chen, *Adv. Mater.*, 2015, **27**, 2775-2782.
13. W. Yin, L. Yan, J. Yu, G. Tian, L. Zhou, X. Zheng, X. Zhang, Y. Yong, J. Li and Z. Gu, *ACS Nano*, 2014, **8**, 6922-6933.
14. L. Cheng, K. Yang, Q. Chen and Z. Liu, *ACS Nano*, 2012, **6**, 5605-5613.
15. X. Liang, Y. Li, X. Li, L. Jing, Z. Deng, X. Yue, C. Li and Z. Dai, *Adv. Funct. Mater.*, 2015, **25**, 1451-1462.
16. J. F. Lovell, C. S. Jin, E. Huynh, H. Jin, C. Kim, J. L. Rubinstein, W. C. W. Chan, W. Cao, L. V. Wang and G. Zheng, *Nat. Mater.*, 2011, **10**, 324-332.
17. L. Cheng, W. He, H. Gong, C. Wang, Q. Chen, Z. Cheng and Z. Liu, *Adv. Funct. Mater.*, 2013, **23**, 5893-5902.
18. M. Zheng, C. Yue, Y. Ma, P. Gong, P. Zhao, C. Zheng, Z. Sheng, P. Zhang, Z. Wang and L. Cai, *ACS Nano*, 2013, **7**, 2056-2067.
19. J. Lin, S. Wang, P. Huang, Z. Wang, S. Chen, G. Niu, W. Li, J. He, D. Cui and G. Lu, *ACS Nano*, 2013, **7**, 5320-5329.
20. J. Yu, C. Yang, J. Li, Y. Ding, L. Zhang, M. Z. Yousaf, J. Lin, R. Pang, L. Wei, L. Xu, F. Sheng, C. Li, G. Li, L. Zhao and Y. Hou, *Adv. Mater.*, 2014, **26**, 4114-4120.
21. H. Liu, D. Chen, L. Li, T. Liu, L. Tan, X. Wu and F. Tang, *Angew. Chem., Int. Ed.*, 2011, **123**, 921-925.
22. J. Shen, L. Zhao and G. Han, *Adv. Drug Delivery Rev.*, 2013, **65**, 744-755.
23. H. Yan, C. Teh, S. Sreejith, L. Zhu, A. Kwok, W. Fang, X. Ma, K. T. Nguyen, V. Korzh and Y. Zhao, *Angew. Chem., Int. Ed.*, 2012, **51**, 8373-8377.
24. S. Gai, C. Li, P. Yang and J. Lin, *Chem. Rev.*, 2014, **114**, 2343-2389.
25. R. Lv, P. Yang, F. He, S. Gai, C. Li, Y. Dai, G. Yang and J. Lin, *ACS Nano*, 2015, **9**, 1630-1647.
26. P. E. Huber, J. W. Jenne, R. Rastert, I. Simiantonakis, H.-P. Sinn, H.-J. Strittmatter, D. von Fournier, M. F. Wannenmacher and J. Debus, *Cancer Res.*, 2001, **61**, 8441-8447.
27. J. F. Schenck, F. A. Jolesz, P. B. Roemer, H. E. Cline, W. E. Lorensen, R. Kikinis, S. G. Silverman, C. J. Hardy, W. D. Barber and E. T. Laskaris, *Radiology*, 1995, **195**, 805-814.
28. G. Chen, H. Qiu, P. N. Prasad and X. Chen, *Chem. Rev.*, 2014, **114**, 5161-5214.

Nanoscale Accepted Manuscript

29. Y. Tao, M. Li, J. Ren and X. Qu, *Chem. Soc. Rev.*, 2015.
30. R. Lv, G. Yang, F. He, Y. Dai, S. Gai and P. Yang, *Nanoscale*, 2014, **6**, 14799-14809.
31. M. L. James and S. S. Gambhir, *Physiol. Rev.*, 2012, **92**, 897-965.
32. Z. Li, S. Yin, L. Cheng, K. Yang, Y. Li and Z. Liu, *Adv. Funct. Mater.*, 2014, **24**, 2312-2321.
33. J. Xie, G. Liu, H. S. Eden, H. Ai and X. Chen, *Acc. Chem. Res.*, 2011, **44**, 883-892.
34. K. Yang, G. Yang, L. Chen, L. Cheng, L. Wang, C. Ge and Z. Liu, *Biomaterials*, 2015, **38**, 1-9.
35. X. R. Song, X. Wang, S. X. Yu, J. Cao, S. H. Li, J. Li, G. Liu, H. H. Yang and X. Chen, *Adv. Mater.*, 2015. **27**, 3285-3291.
36. B. Yuan, X. Hou, Y. Han, W. Luan and S.-t. Tu, *New J. Chem.*, 2012, **36**, 2101-2105.
37. S. Thanikaikarasan, T. Mahalingam, K. Sundaram, A. Kathalingam, Y. Deak Kim and T. Kim, *Vacuum*, 2009, **83**, 1066-1072.
38. X. Mao, J.-G. Kim, J. Han, H. S. Jung, S. G. Lee, N. A. Kotov and J. Lee, *J. Am. Chem. Soc.*, 2014, **136**, 7189-7192.
39. C. W. Jung and P. Jacobs, *Magn. Reson. Imaging*, 1995, **13**, 661-674.
40. L. Cheng, K. Yang, Y. Li, J. Chen, C. Wang, M. Shao, S. T. Lee and Z. Liu, *Angew. Chem., Int. Ed.*, 2011, **123**, 7523-7528.
41. K. Yang, S. Zhang, G. Zhang, X. Sun, S.-T. Lee and Z. Liu, *Nano Lett.*, 2010, **10**, 3318-3323.
42. T. Liu, C. Wang, X. Gu, H. Gong, L. Cheng, X. Shi, L. Feng, B. Sun and Z. Liu, *Adv. Mater.*, 2014, **26**, 3433-3440.
43. J. Yao, L. Wang, C. Li, C. Zhang and L. V. Wang, *Phys. Rev. Lett.*, 2014, **112**, 014302.
44. J.-M. Yang, C. Favazza, R. Chen, J. Yao, X. Cai, K. Maslov, Q. Zhou, K. K. Shung and L. V. Wang, *Nat. Med.*, 2012, **18**, 1297-1302.
45. W. Cai and X. Chen, *J. Nucl. Med.*, 2008, **49**, 113S-128S.

Nanoscale Accepted Manuscript

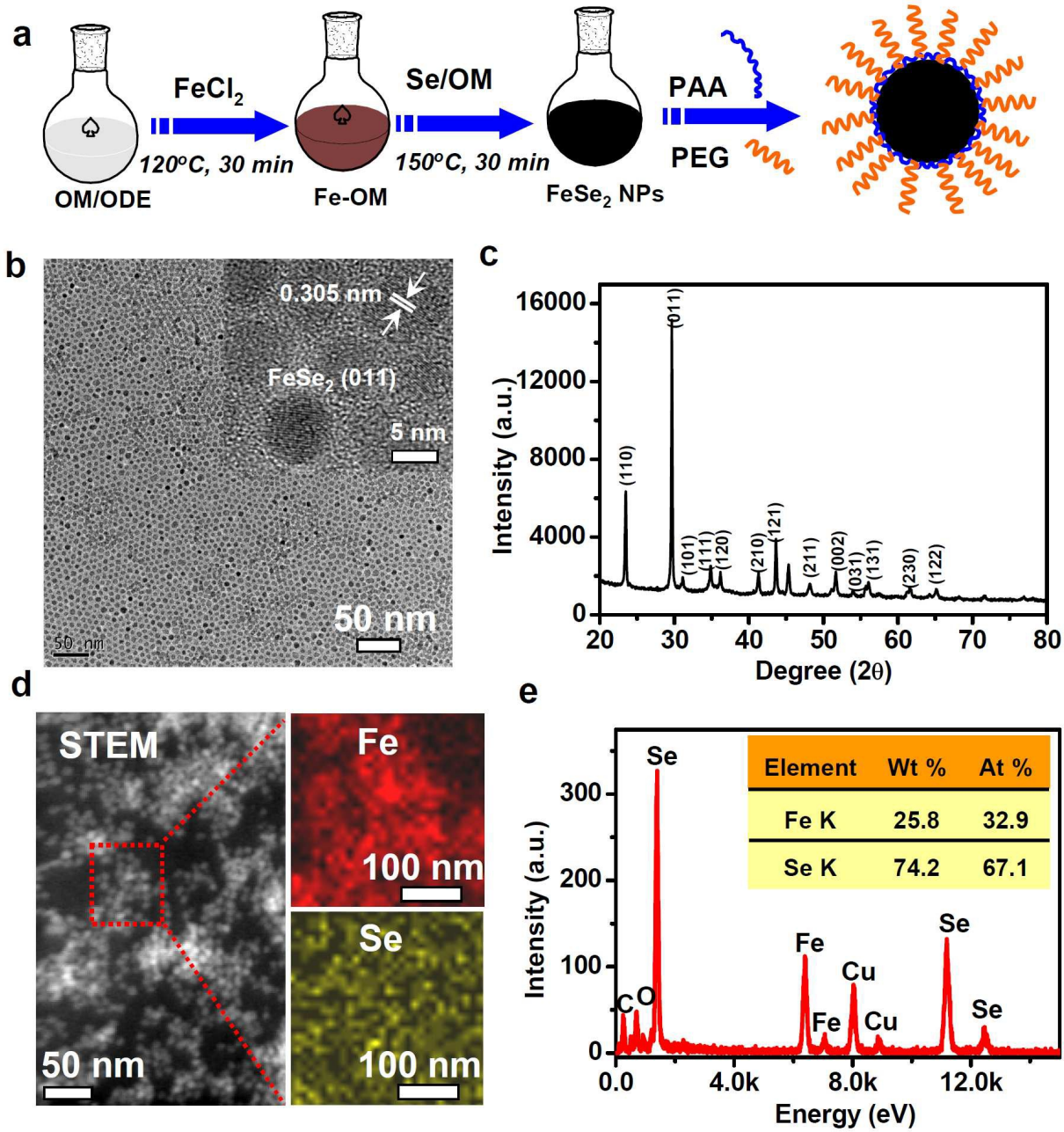

Figure 1. Synthesis and characterization of $FeSe_2$ nanoparticles. (**a**) A scheme showing fabrication process of $FeSe_2$-PEG nanoparticles. (**b**) A TEM image of $FeSe_2$ nanoparticles. Inset: A high-resolution TEM image of $FeSe_2$ nanoparticles. (**c**) XRD spectrum of as-made $FeSe_2$ nanoparticles. (**d**) STEM-EDS-mapping of $FeSe_2$ nanoparticles. (**e**) EDX pattern of the $FeSe_2$ samples. The inset table presents the elemental ratios (weight and atom percentages) calculated by the EDX software (K-shell intensity ratios are indicated).

Nanoscale Accepted Manuscript

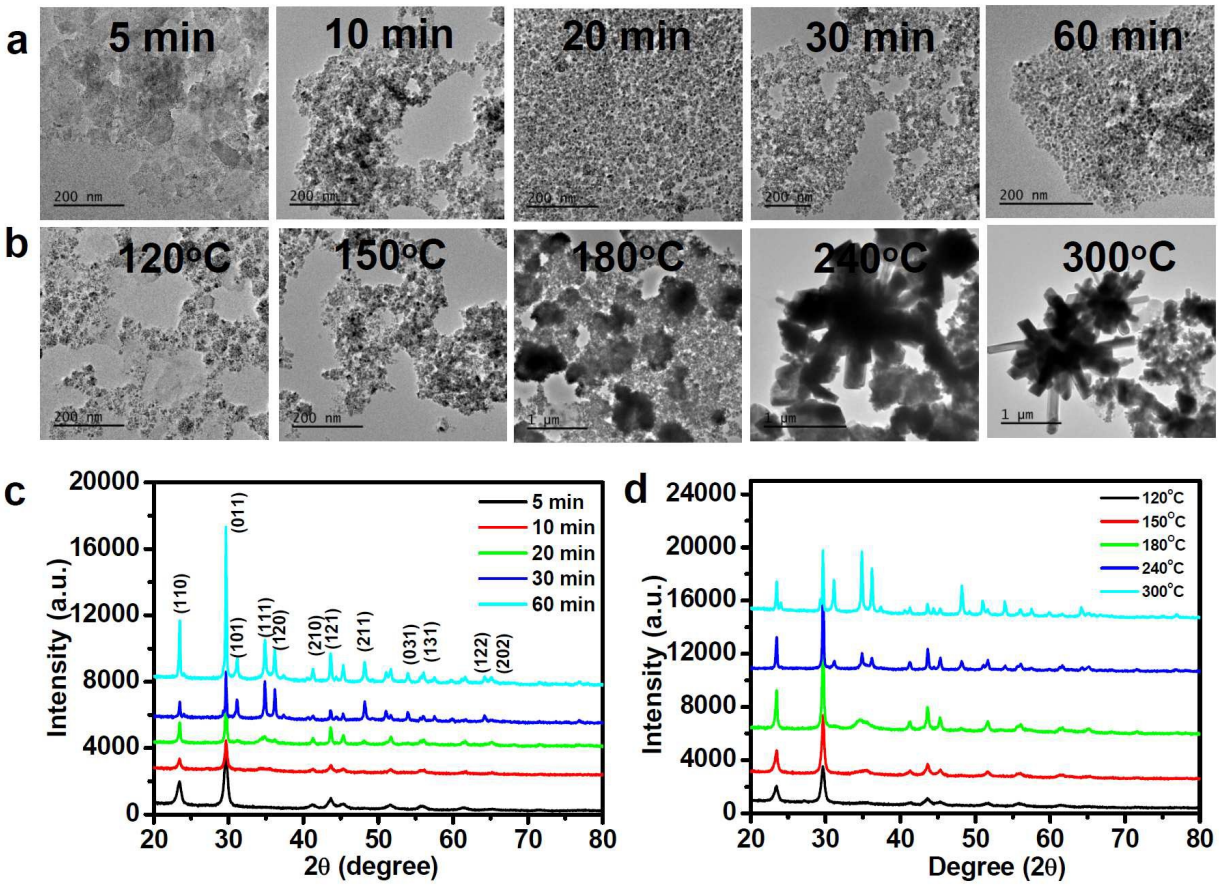

Figure 2. Control experiments for the synthesis of $FeSe_2$ nanoparticles. (**a&b**) TEM images of $FeSe_2$ nanoparticles prepared at different reaction time (**a**) (5min, 10 min, 20 min, 30 min, and 60 min) at 150°C, and under different reaction temperatures (**b**) (120 °C, 150 °C, 180 °C, 240 °C, and 300 °C) for 30 min. (**c&d**) XRD spectra of $FeSe_2$ nanoparticles prepared at different reaction time (**c**) (5min, 10 min, 20 min, 30 min, and 60 min) at 150°C, and different reaction temperatures (**d**) (120 °C, 150 °C, 180 °C, 240 °C, and 300 °C) for 30 min.

Nanoscale Accepted Manuscript

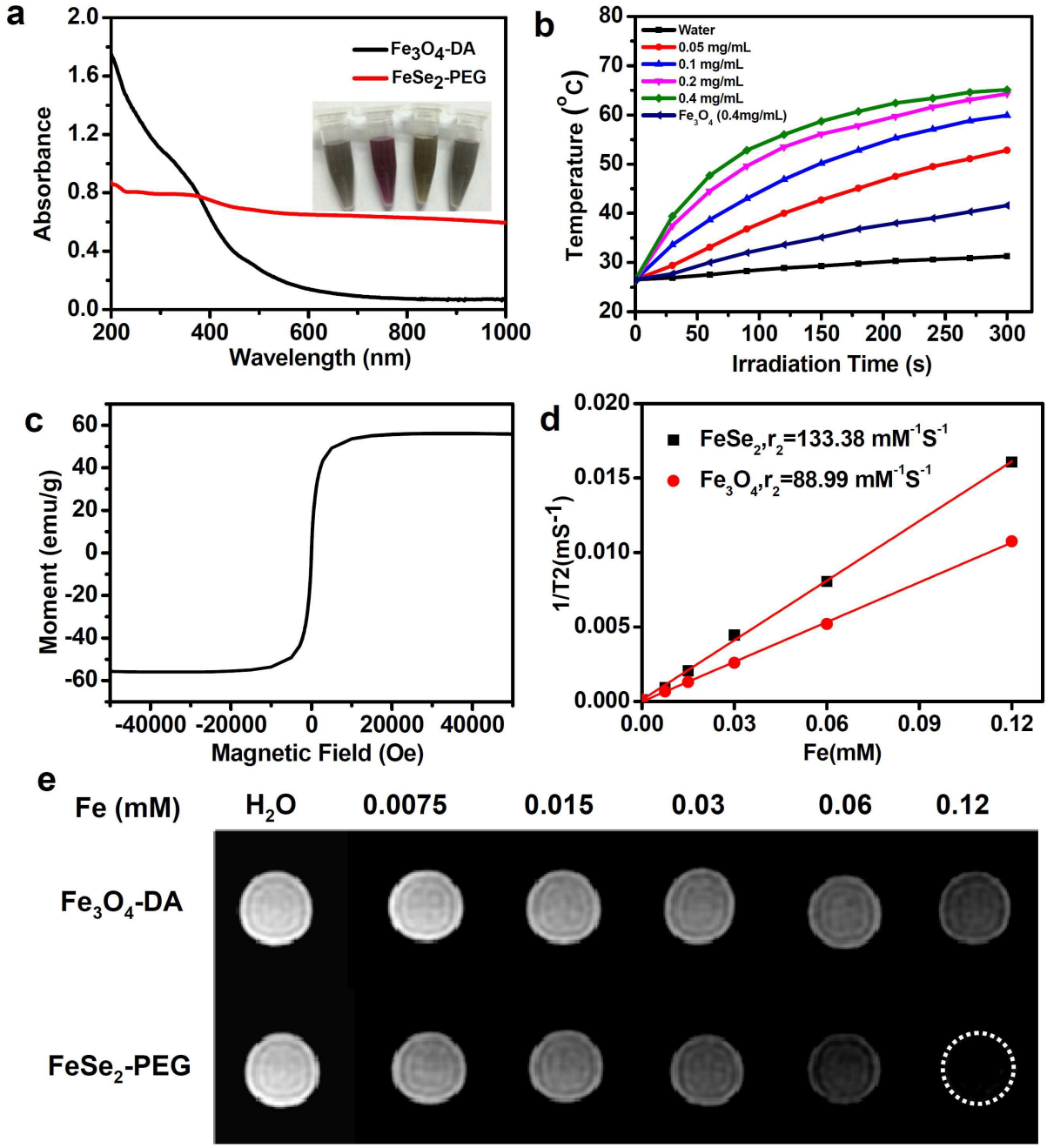

Figure 3. Optical and magnetic properties of $FeSe_2$-PEG nanoparticles. (**a**) UV-vis-NIR absorbance spectra of $FeSe_2$-PEG and Fe_3O_4-DA at the same concentration (0.04 mg/mL). Inset: A photo of $FeSe_2$-PEG in various solutions (From left to right: water, phosphate buffered saline, RMPI-1640 cell medium, and fetal bovine serum). $FeSe_2$-PEG exhibited excellent stability in all tested physiological solutions. (**b**) Heating curves of $FeSe_2$-PEG solutions at different concentrations and Fe_3O_4-DA solution at 0.4 mg/mL under irradiation by an 808-nm laser (0.8 W cm^2) for 5 min. (**c**) Magnetization loops of $FeSe_2$-PEG at room temperature. (**d&e**) The relative relaxation rate R2 (**d**) and T2-weighted MR images (**e**) of $FeSe_2$-PEG and Fe_3O_4-DA solutions at different Fe concentrations.

Nanoscale Accepted Manuscript

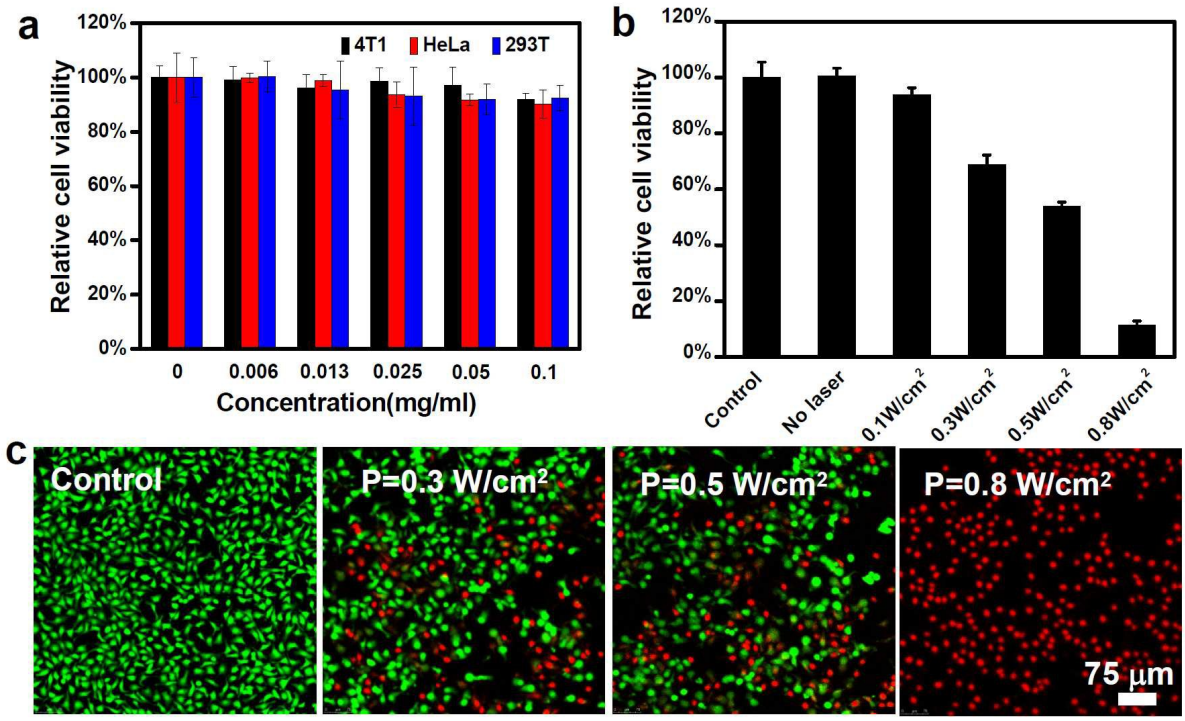

Figure 4. *In vitro* cell experiments. (**a**) Relative viabilities of 4T1, HeLa, and 293T cells after being incubated with various concentrations of $FeSe_2$-PEG for 24 h. $FeSe_2$-PEG appeared to be not obviously toxic. (**b**) Relative viabilities of 4T1 cells after incubation with $FeSe_2$-PEG under 808 nm laser irradiation for 5 min with different laser power densities. Error bars were based on the standard deviations (SD) of six parallel samples. (**c**) Confocal fluorescence images of Calcein AM/PI co-stained 4T1 cells after incubation with $FeSe_2$-PEG and being exposed to the 808-nm laser at different laser power densities.

Nanoscale Accepted Manuscript

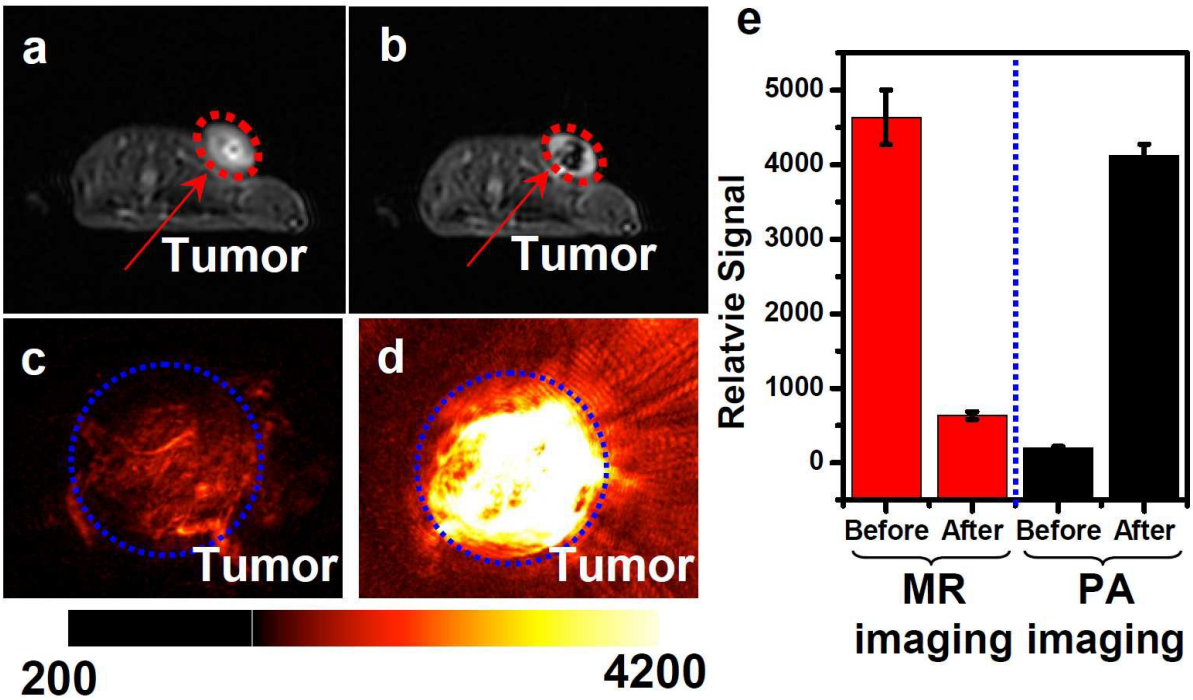

Figure 5. *In vivo* dual-modal imaging. (**a&b**) MR images of mice before and after *i.t.* injection with $FeSe_2$-PEG (40 μL, 2 mg/mL). (**c&d**) PA images of tumors on mice before and after i.t. injection with $FeSe_2$-PEG (40 μL, 2 mg/mL). (**e**) The relative T2 signals and photoacoustic signals in the tumors from mice before and after *i.t.* injection of $FeSe_2$-PEG.

Nanoscale Accepted Manuscript

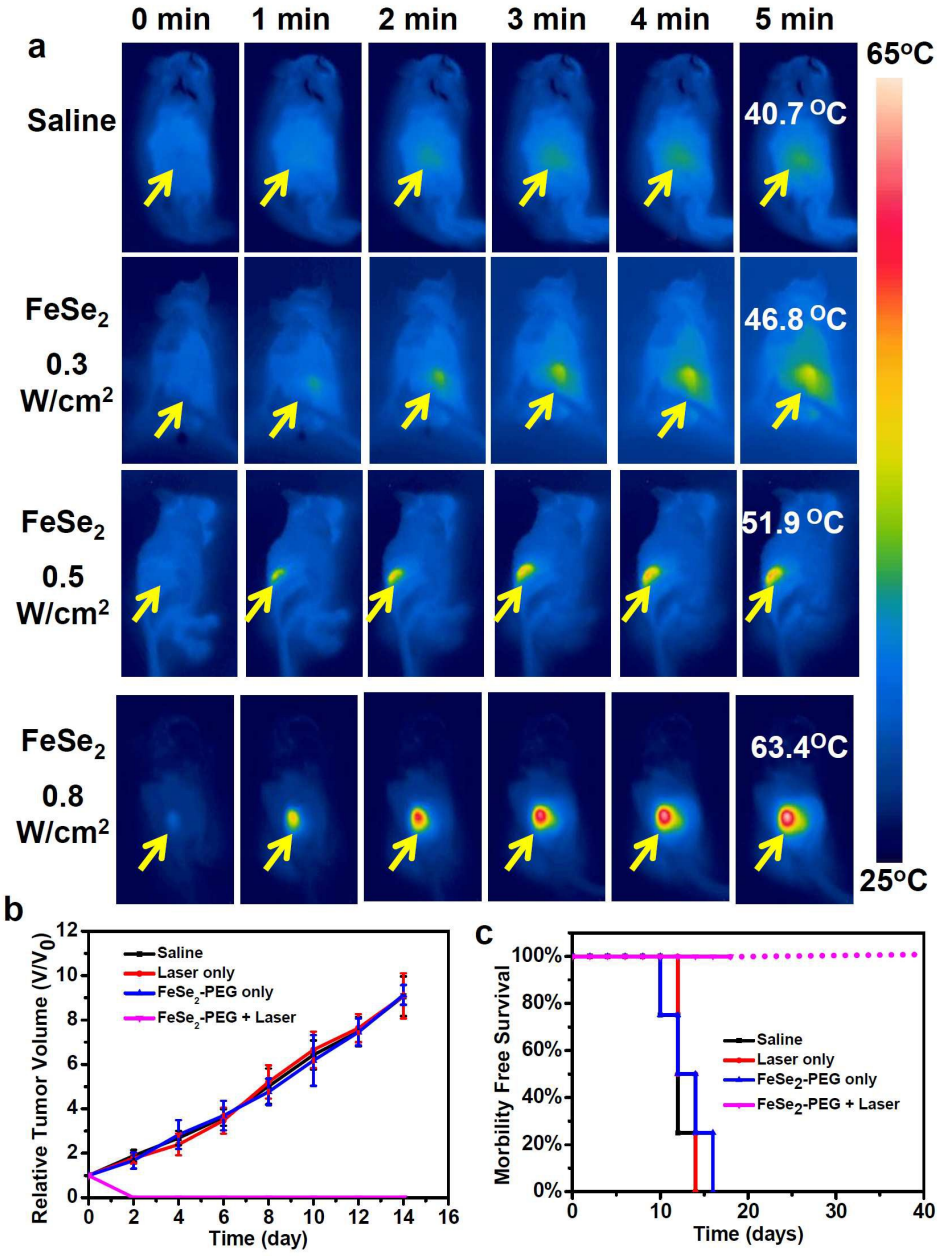

Figure 6. *In vivo* PTT. (**a**) IR thermal images of 4T1 tumor-bear mice with *i.t.* injection of $FeSe_2$-PEG (dose=4 mg/kg, irradiated at 0.5 h p.i.) under the 808-nm laser irradiation taken at the different laser power densities (0.3, 0.5 and 0.8 W/cm^2) for 5 min. Tumor-bearing mice *i.t* injected with the same volume of saline were also exposed to the 808-nm laser (0.8W/cm^2) as the control. (**b**) Relative tumor volume curves of different groups of mice after the various treatments. Four groups of mice were used: saline (n = 4) only without laser; laser only without $FeSe_2$-PEG injection (n = 4); injection of $FeSe_2$-PEG without laser irradiation (n =4), and injection of $FeSe_2$-PEG with 808-nm laser irradiation at the power density of 0.8 W/cm^2 for 5 min (n=4). Error bars were based on standard errors of the mean (SEM). **(c)** Survival curves of mice after various treatments as indicated in (**b**).

Nanoscale Accepted Manuscript

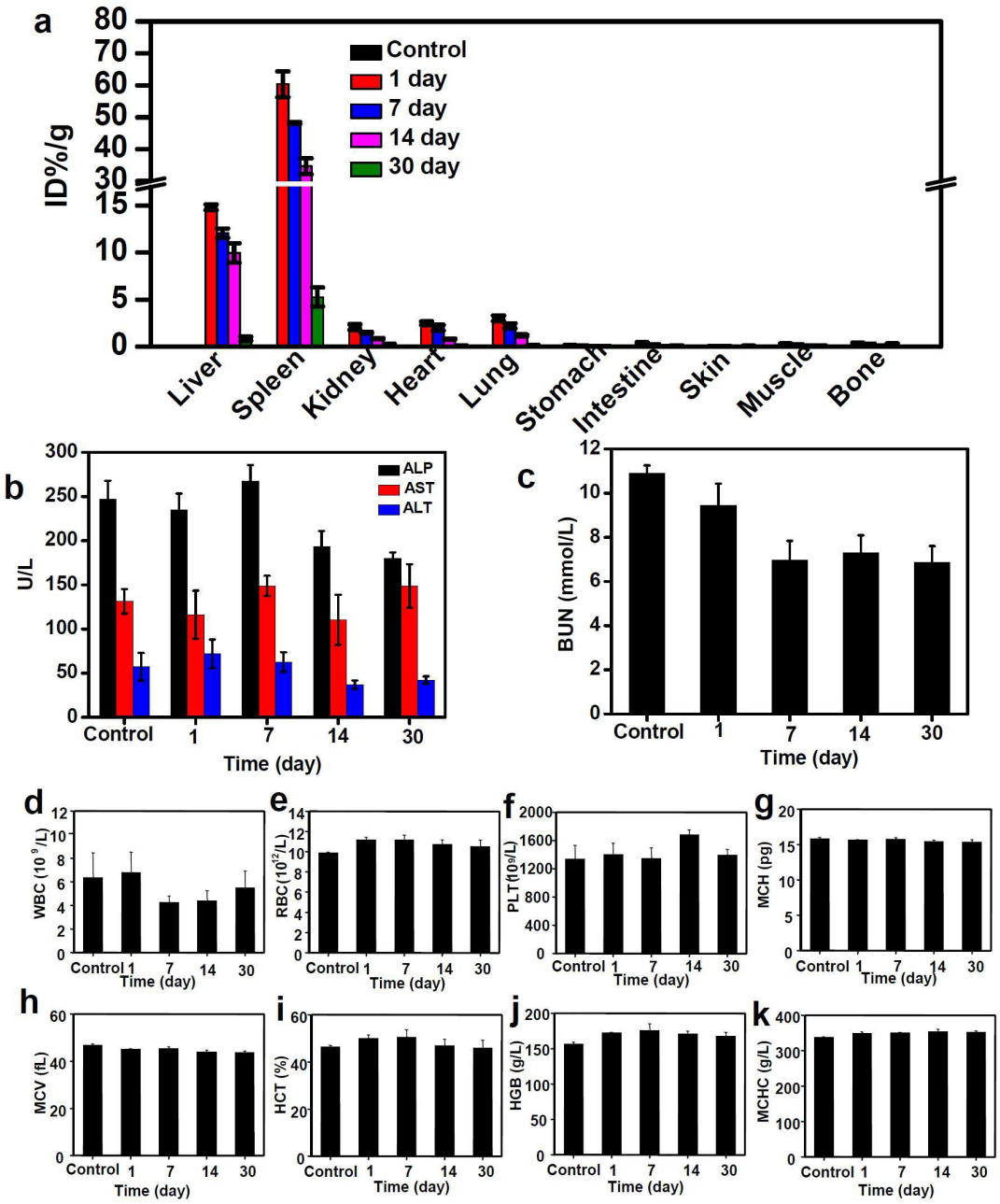

Figure 6. Biodistribution and *in vivo* long-term toxicology studies of $FeSe_2$-PEG in healthy Blab/c mice. (**a**) Biodistribution of $FeSe_2$-PEG in mice at different time points (1, 7, 14, and 30 days) post-injection measured by ICP-AES (Fe levels). (**b-k)** Blood biochemistry and hematology data of female Balb/c mice treated with $FeSe_2$-PEG at the dose of 20 mg/ kg. Four mice without injection were used as the un-treated control. (**b**) ALT, ALP and AST levels in the blood at various time points after $FeSe_2$-PEG treatment. (**c**) Blood urea nitrogen (BUN) levels overtime. (**d-k**) Time course changes of white blood cells (WBC, **d**), red blood cells (RBC, **e**), platelets (PLT, **f**), mean corpuscular hemoglobin (MCH, **g**), mean corpuscular volume (MCV, **h**), hematocrit (HCT, **i**), haemoglobin (HGB, **j**), and mean corpuscular hemoglobin concentration (MCHC, **k**) from control mice and $FeSe_2$-PEG treated mice. Statistics were based on four mice per data point.

Nanoscale Accepted Manuscript